**Supporting information**

# Periodic Silver and Gold Nanodot Array Fabrication on Nanosphere Lithography-Based Patterns Using Electroless Deposition

**Authors:** Sasanka B. Ulapane, Nilan J. B. Kamathewatta, Ashley K. Borkowski, Samuel J. Steuart, Cindy L. Berrie*

Department of Chemistry, University of Kansas, Lawrence, Kansas 66045

Corresponding author: cberrie@ku.edu

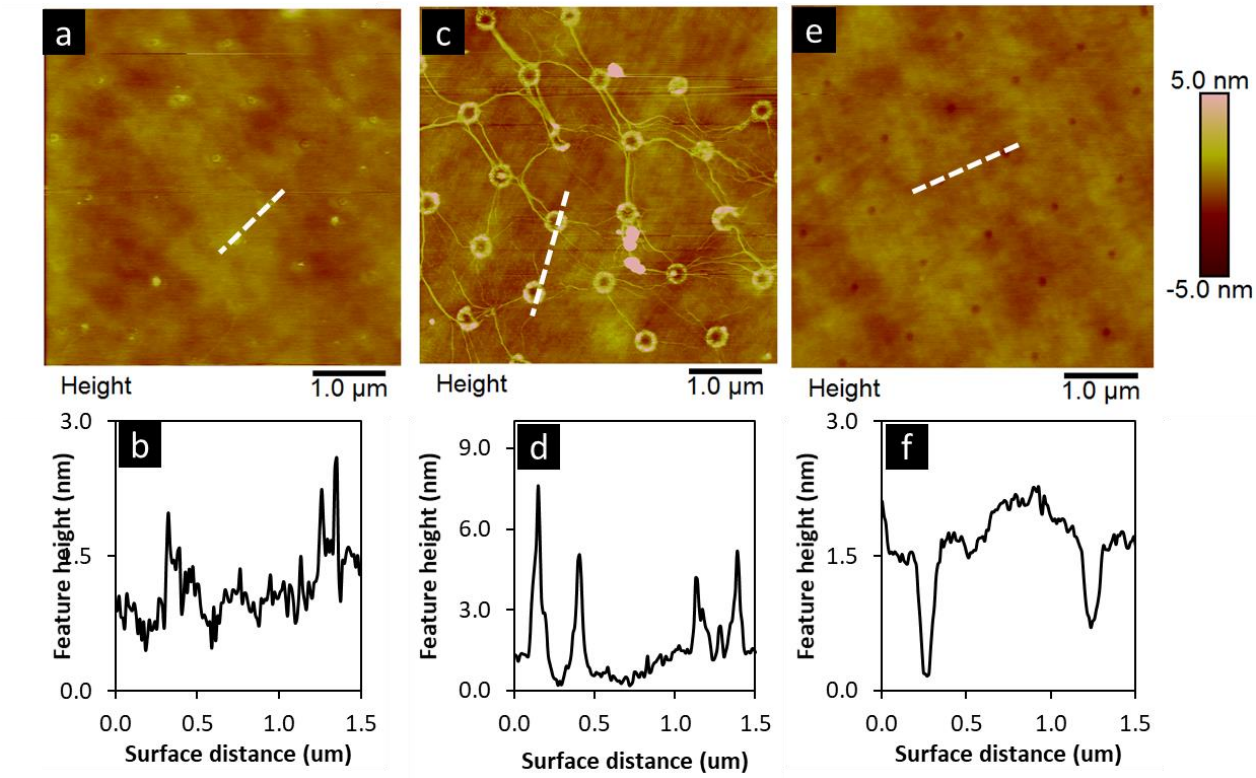


***Figure S1:*** *AFM images of nanopore arrays on OTS monolayers formed by 1000 nm nanospheres, after nanospheres drop-cast on Si wafer samples were dried under different humidity conditions. (a) Under low humidity (<20%). (b) Cross section of (a) along the dotted line. (c) Under higher humilities (40-68%). (d) Cross section of (c) along the dotted line. (e) After fully drying the surface under ambient conditions (~22 °C and ~22% relative humidity) for 30 minutes before being oven dried at 100 °C for 1 hr and re-hydrating the surface to 60-70% humidity using a sealed bag to control the humidity by bubbling $N_2$ through water. (f) Cross section of (e) along the dotted line. All samples were submerged in 2.5 mM OTS in toluene solutions for 24 hrs after different drying step to form an OTS monolayer.*

Residual water on the $SiO_2$ surface plays a critical role in the monolayer formation process and, consequently, in this fabrication approach.[1] The exchange of chloro groups on OTS molecules with hydroxyl groups is vital for the water-dependent self-assembly process. To investigate the effect of water, substrates were dried under varying humidity conditions. Garno *et. al.* [2] previously demonstrated[3] that the relative humidity at which the samples are dried prior to monolayer formation affects the quality, packing, and thickness of the monolayer formed on the $SiO_2$ surface.[2]

Here, three different drying conditions were explored: (1) low humidity, long duration drying, (2) higher humidity or shorter duration drying, and (3) complete drying of the surface and rehydration in a glove bag at 70% humidity for an hour. Monolayer formation at 70% relative humidity after oven drying reproducibly resulted in a pore depth consistent with literature values[4,5] of monolayer thickness, without obvious polymerization on the surface. Figure S1 shows nanopore arrays made under different humidity conditions along with cross-sections across fabricated features. The expected nanopore patterns were rarely observed in the low humidity trials, suggesting the lack of water on the surface inhibits silanization on surface (Figure S1a). Shorter drying durations (or higher humidity) left traces of pores and ring like structures (Figure S1b) that correlate with the nanosphere packing. This was previously reported[6,7,5] to be a result of trapped residual water on the edges of nanosphere contact points, creating a water meniscus between the substrate and nanosphere. Formation of a well-packed OTS monolayer on the exposed area of the $SiO_2$ requires a uniformly adsorbed residual water layer. This was achieved by allowing samples to dry under ambient conditions before completely drying substrates in an oven followed by rehydrating at 60-70% relative humidity in a sealed bag to control humidity. Controlling the relative humidity establishes an equilibrium between surface adsorbed and gas phase water at a given temperature. Relative humidity in the bag during monolayer formation was controlled by adjusting the rate of $N_2$ bubbled through a temperature-controlled water container into the bag. The substrates were equilibrated at controlled humidity for approximately one hour.

AFM images of the nanopore platforms were taken at 10 x 10 $\mu m^2$ sizes using scan rates of 2.0-2.5 Hz. Further decreasing the scan rate to 0.5 Hz did not significantly improve the quality of the images collected. Diameter measurements are not corrected for possible AFM tip convolution effects that could occur when imaging confined pore like structures during this study.

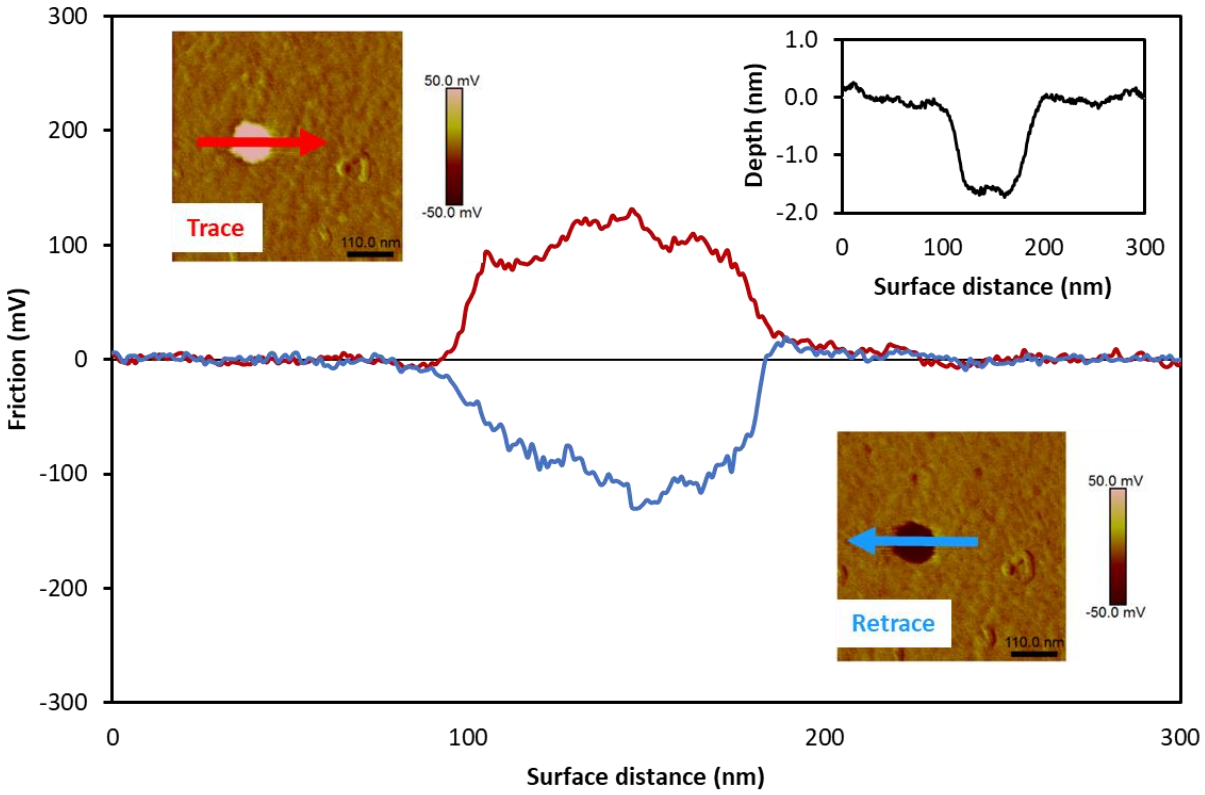


***Figure S2:*** *Lateral force images of trace (top left) and retrace (bottom right) signals over a nanopore produced from 500 nm spheres. Graph represents the magnitude and contrast of the signal across the blue and red arrows on trace and retrace images. Topography profile of the pore is shown on the top right.*

Electroless metal reduction on Si surfaces and etching of oxide layer

$$NH_4F(aq) + H_2O(l) \leftrightharpoons NH_4^+(aq) + F^-(aq) \quad (1)$$

$$F^-(aq) + H_3O^+(aq) \leftrightharpoons HF(aq) + H_2O(l) \quad (2)$$

$$SiO_2(S) + 6HF(aq) \rightarrow 2H^+(aq) + SiF_6^{2-}(aq) + 2H_2O(l) \quad (3)$$

$$Si(s) + 6F^-(aq) \rightarrow SiF_6^{2-}(aq) + 4e^- \quad (4)$$

$$M^{+n}(aq) + ne^-(aq) \rightarrow M(s) \quad (5)$$

***SI Scheme 1:*** *Redox reactions between silicon substrate and metal ions. (1) dissociation of $NH_4F$, (2) formation of HF from $F^-$ ions produced from $NH_4F$, (3) removal of $SiO_2$ by HF etching, (4) oxidation of Si, and (5) reduction of metal ions where $M^{n+} = Ag^+$ or $Au^{3+}$.*

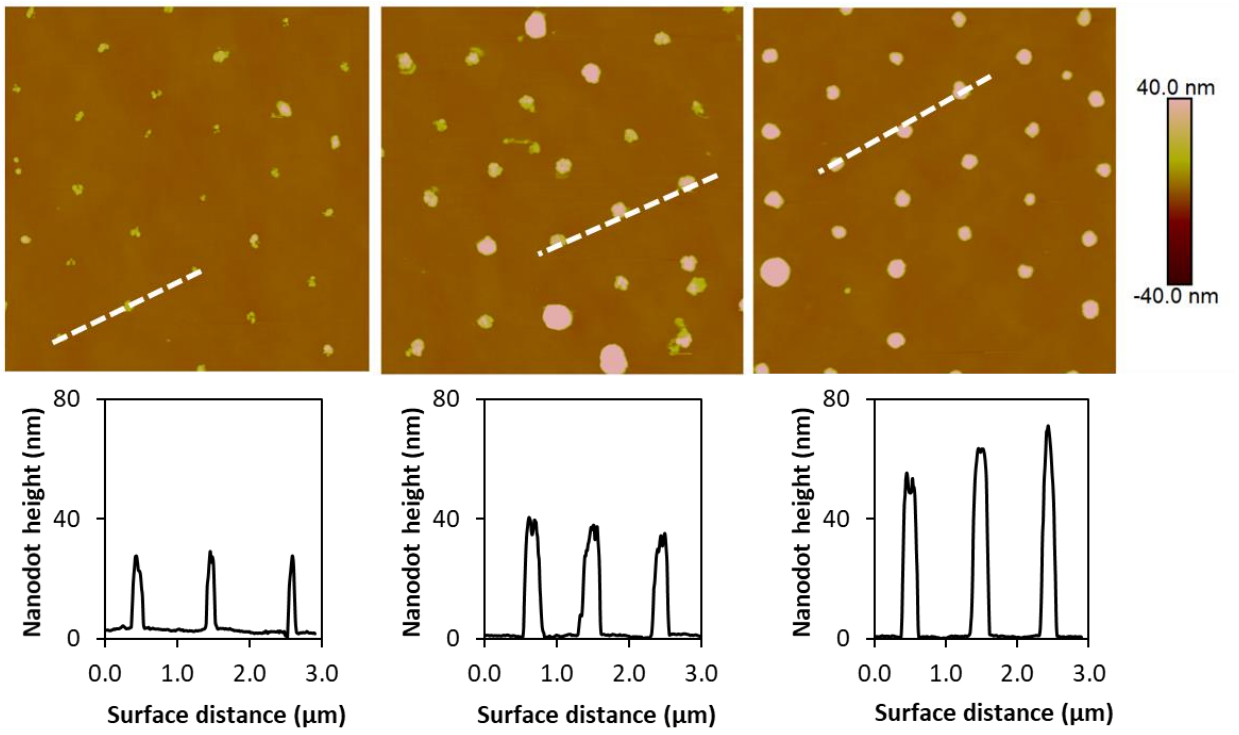


***Figure S3: Au*** *nanodots grown in nanopore arrays spaced 1000 nm apart for 30, 60, 90 s in standard gold plating solution after a 30s pre-etching step in 5% $NH_4F$. Standard gold plating solution (0.002 M $HAuCl_4$ and 0.02 M $NH_4F$).*

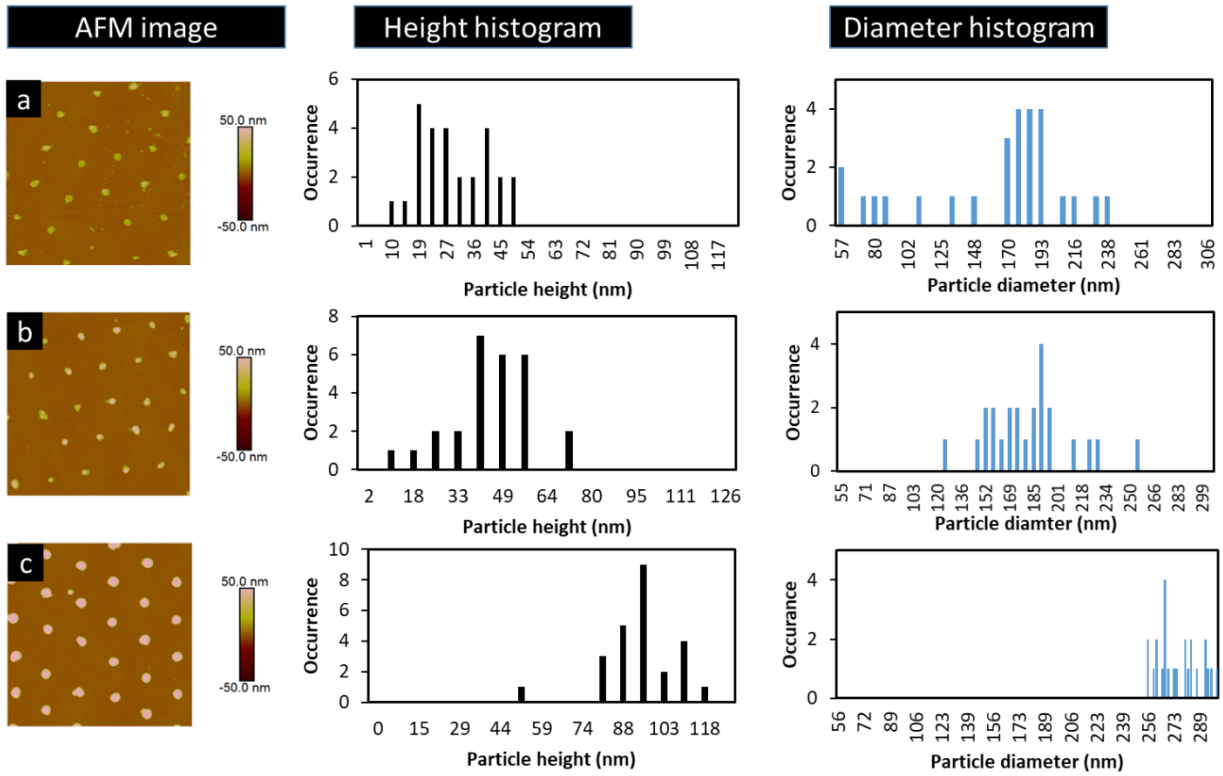


***Figure S4:*** *Representative AFM images of* ***Ag*** *nanodots made using different plating durations (a) 10, (b) 15, (c) 30 s, on nanopores spaced 1000 nm. Each time point is presented with respective height and diameter histograms for n>50 dots. Nanopore patterns were pre etched in 5% W/W $NH_4F$ for 30 s before silver plating was performed in a silver plating solution containing 0.02 M $NH_4F$ and 0.01 M $AgNO_3$ for specified times.*

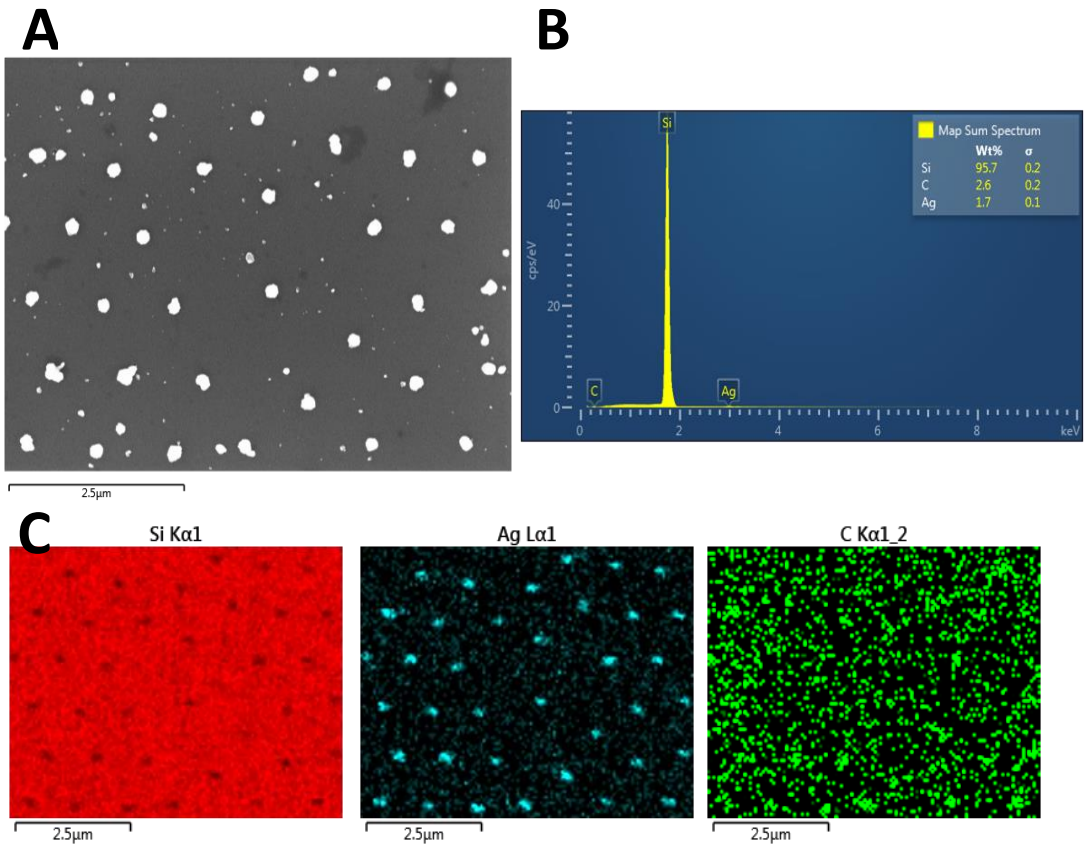


***Figure S5:*** *SEM and EDS data collected on* ***Ag*** *nanodot sample fabricated from 1.0 µM spheres. A) SEM image of* ***Ag*** *dots on Si(111) surface coated with OTS monolayer B) elemental characterization from image in (A) using EDS, and C) Compositional mapping for Si, Ag, and C from the same spot as image in (A) showing the Ag is localized to the fabricated dots with 1.0 µm spacing.*

For elemental characterization, SEM and EDS measurements were carried out on a representative sample. The sample was mounted on aluminum stub with sticky carbon tabs. A SU8230 Scanning Electron Microscope (Hitachi Ltd., Japan) with a silicon drift EDS detector (Oxford Instruments, X-MaxN, UK) was used to measure the surface morphology, elemental composition and distribution of elements. All the SEM data reported were obtained at an acceleration voltage of 10kV and the images were collected with a Secondary Electron detector. The elemental mapping and energy spectrums were acquired with Aztec tools (Oxford Instruments, UK). The elemental maps of the element indicate the presence of Ag elements patterned on a silicon substrate.

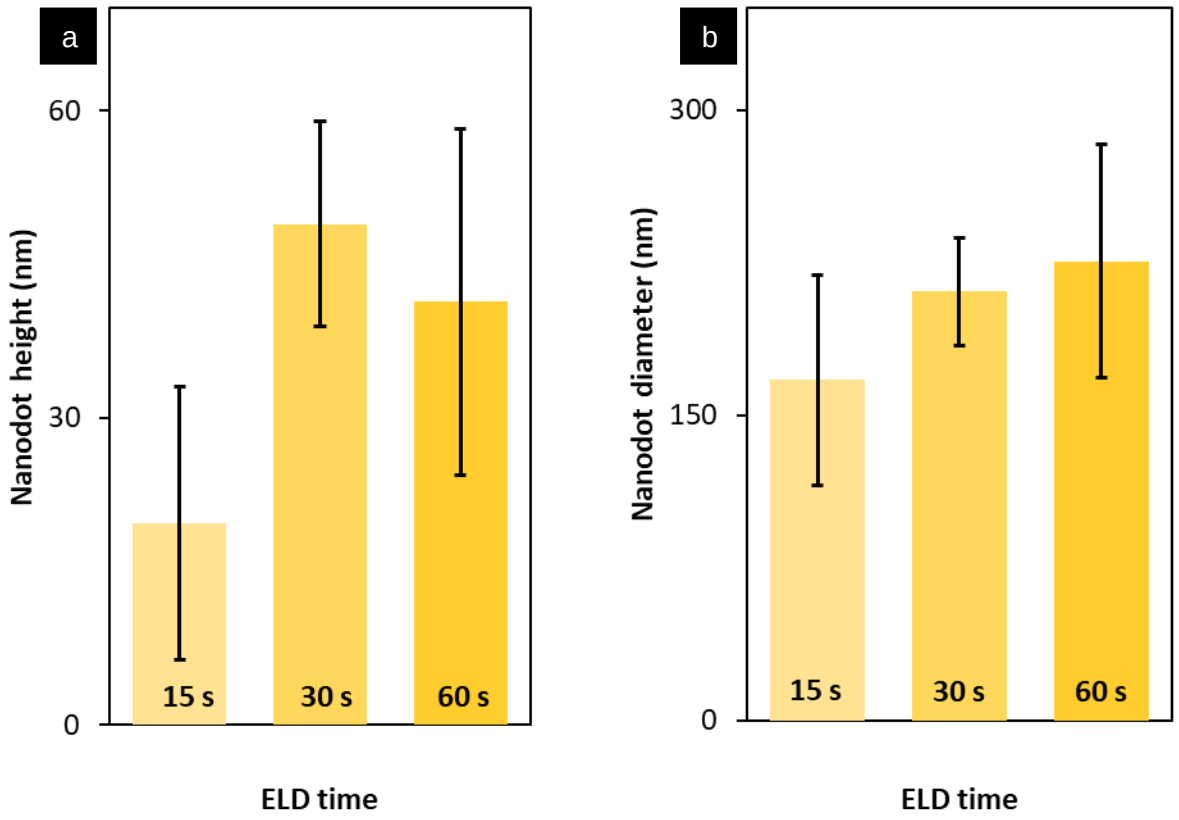


***Figure S6:*** *(a) Nanodot height and (b) nanodot diameter variation after electroless deposition of Ag for 15, 30, 60 s* ***without employing a pre-etching step*** *prior to ELD. Standard plating conditions of 0.01 M $AgNO_3$ and 0.02 M $NH_4F$ were employed for ELD for each plating duration.*

Electroless deposition was performed excluding the pre-etching step. Here, it was observed that the metal nanodots can be grown on nanopores without the pre-etching step, utilizing $NH_4F$ in the plating solution to etch the $SiO_2$ layer. However, the size distribution of the nanodots grown without the pre-etching step at a given time point was broader compared to that of the nanodots grown with the pre-etching step. This can be explained by the even removal of the oxide film by $NH_4F$ pre-etching step, prior to metal plating, facilitating faster and uniform growth of a seed layer in nanopores.

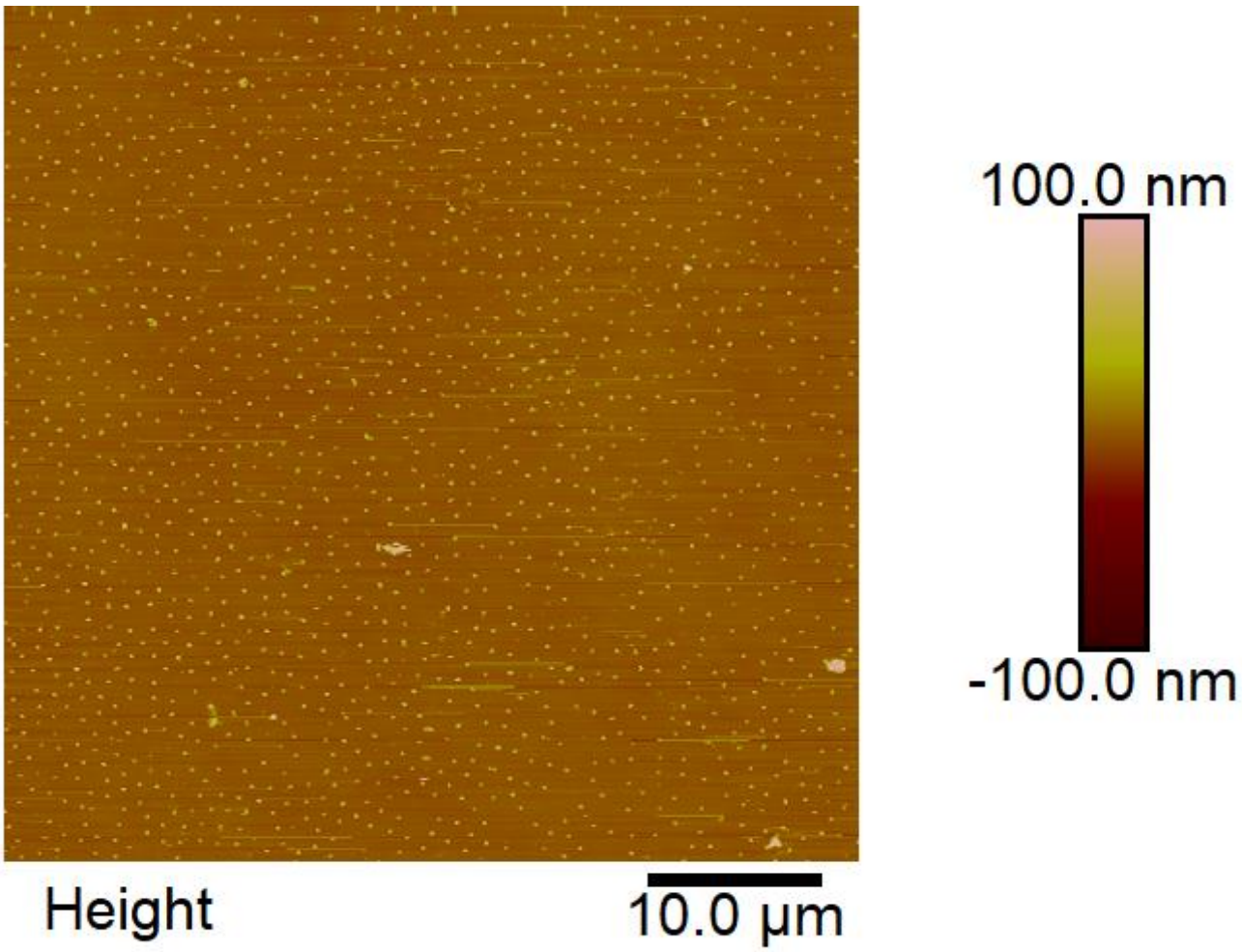


***Figure S7:*** *1000 nm apart Ag nanodots in a 50 x 50 µm$^2$ area. Standard plating conditions of 0.01 M $AgNO_3$ and 0.02 M $NH_4F$ were employed for ELD after 30 s pre-etching in 5% w/w $NH_4F$.*

## References


(1) Desbief, S.; Patrone, L.; Goguenheim, D.; Guerin, D.; Vuillaume, D. Impact of Chain Length , Temperature , and Humidity on the Growth of Long Alkyltrichlorosilane Self-Assembled Monolayers W. *Phys. Chem. Chem. Phys.* **2011**, *13*, 2870–2879. https://doi.org/10.1039/c0cp01382j.

(2) Li, J.; Lusker, K. L.; Yu, J.; Garno, J. C. Engineering the Spatial Selectivity of Surfaces at the Nanoscale Using Particle Lithography Combined with Vapor Deposition of Organosilanes. *ACS Nano* **2009**, *3* (7), 2023–2035.

(3) Highland, Z. L.; Saner, C. K.; Garno, J. C. Preparation of Octadecyltrichlorosilane Nanopatterns Using Particle Lithography: An Atomic Force Microscopy Laboratory. *J. Chem. Educ.* **2018**, *95*, 320–325. https://doi.org/10.1021/acs.jchemed.7b00158.

(4) Brownfield, A. L.; Causey, C. P.; Mullen, T. J. Influence of Solvent on Octadecyltrichlorosilane Nanostructures Fabricated Using Particle Lithography. *J. Phys. Chem. C* **2015**, *119* (22), 12455–12463. https://doi.org/10.1021/acs.jpcc.5b02576.

(5) Brown, A. L.; Causey, C. P.; Mullen, T. J. Effects of Surface Water on Organosilane Nanostructure Fabrication Using Particle Lithography. *Thin Solid Films* **2015**, *594*, 184–191. https://doi.org/10.1016/j.tsf.2015.10.029.

(6) Saner, C. K.; Lu, L.; Zhang, D.; Garno, J. C. Chemical Approaches for Nanoscale Patterning Based on Particle Lithography with Proteins and Organic Thin Films. *Nanotechnol Rev* **2015**, *4* (2), 129–143. https://doi.org/10.1515/ntrev-2015-0002.

(7) Kulkarni, S. A.; Lyles, V. D.; Serem, W. K.; Lu, L.; Kumar, R.; Garno, J. C. Solvent-Responsive Properties of Octadecyltrichlorosiloxane Nanostructures Investigated Using Atomic Force Microscopy in Liquid. *Langmuir* **2014**, *30*, 5466–5473.